On the Role of Carbon Radical Insertion Reactions in the Growth of Diamond by Chemical Vapor Deposition Methods

James C. Richley,† Jeremy N. Harvey,* and Michael N. R. Ashfold*

School of Chemistry, University of Bristol, Cantock's Close, Bristol BS8 1TS, U.K.

Received: June 29, 2009; Revised Manuscript Received: August 25, 2009

Potential energy profiles for the insertion of gas phase C atoms, and CH, CH_2, C_2, C_2H, and C_3 radicals, into C−H and C−C bonds on a 2 × 1 reconstructed, H-terminated diamond {100} surface have been explored using both quantum mechanical (density functional theory) and hybrid quantum mechanical/molecular mechanical (QM/MM) methods. Both sets of calculations return minimum energy pathways for inserting a C atom, or a CH(X), C_2(X), or CH_2(a) radical into a surface C−H bond that are essentially barrierless, whereas the barriers to inserting any of the investigated species into a surface C−C bond are prohibitively large. Reactivity at the diamond surface thus parallels behavior noted previously with alkanes, whereby reactant species that present both a filled σ orbital and an empty p(π) orbital insert readily into C−H bonds. Most carbon atoms on the growing diamond surface under typical chemical vapor deposition conditions are H-terminated. The present calculations thus suggest that insertion reactions, particularly reactions involving C(^{3}P) atoms, could make a significant contribution to the renucleation and growth of ultrananocrystalline diamond (UNCD) films.

I. Introduction

Growth of diamond by chemical vapor deposition (CVD) methods is now an established technology which, by judicious choice of process conditions, can yield material with grain sizes ranging from ultrananocrystalline (UNCD) and nanocrystalline (NCD) films, through plates and wafers of microcrystalline (MCD) diamond, to single crystal diamond (SCD). Numerous prior studies have contributed to the development of what is now regarded as the "standard" model of diamond growth by CVD.[1−3] Key elements of this model include the following. The surface of the growing diamond lattice itself is stabilized, and prevented from rearranging to graphitic carbon, by termination with hydrogen atoms (or similar chemical species). The growth temperature (typical substrate temperature, T_{sub}, values are in the range 900−1200 K) is too low for spontaneous bulk rearrangement to occur. Growth relies on the activation (e.g., by a microwave (MW) plasma) of an appropriate gas mixture that, typically, comprises methane (or other hydrocarbon) and hydrogen, supplemented with varying amounts of a rare gas (e.g., argon). Activation causes H_2 dissociation. The resulting H atoms react with the source hydrocarbon and create a complex mixture of hydrocarbon species, including reactive carbon-containing radicals. The H atoms also abstract hydrogen from the surface C−H bonds, thereby creating surface radical sites. Occasionally, a carbon-containing gas phase radical will react with such a radical site, resulting in a chemisorbed carbon species. More frequently, however, the radical sites are simply reterminated by combining with another gas phase H atom. The rapid cycling of the surface H atoms is also crucial in driving the sequences of abstraction/rearrangement/addition steps involved in accommodating adsorbed carbon species into the lattice.

A series of recent papers have reported the use of several complementary techniques to provide a comprehensive analysis of MW activated hydrocarbon/H_2/Ar gas mixtures.[4−6] In situ laser absorption spectroscopy methods have been used to provide absolute column densities of stable hydrocarbons (methane and acetylene) and transient species (e.g., C_2 and CH radicals, and electronically excited H atoms) as functions of process conditions (e.g., hydrocarbon source gas, input gas mixing ratios, input power, P and total pressure, p) and height (z) above the substrate surface.[4,5] Spectral analysis has also provided a measure of the local gas temperature (T_{gas}) in the regions where these various species have their maximal concentrations. Spatially resolved optical emission studies have provided further (relative) measures of these (and other) species, and insights into the electronic properties of the plasma (e.g., the electron number density, n_e, and temperature T_e).[6] The measurements have been complemented by sophisticated 2-D (r, z for the cylindrically symmetric reactors of interest) modeling of the relevant plasma-chemical processes,[7] with the experimental measurements and the model outputs serving to test and tension each other in a symbiotic manner.

This combined approach has served to reaffirm the importance of the families of fast "H-shifting" reactions 1 and 2 in activating the input CH_4, e.g., in the hot regions, via abstraction reactions of the form

$$CH_y + H \rightleftharpoons CH_{y-1} + H_2 \qquad y = 4-1 \qquad (1)$$

and, in the cooler regions, by addition reactions

$$CH_{y-1} + H(+M) \rightleftharpoons CH_y(+M) \qquad y = 4-1 \qquad (2)$$

(where M is a third body). Gas phase C_2H_x species are formed by CH_y radical recombinations, e.g.

* Authors for correspondence. Tel: +44 117 9288312/+44 117 9546991. Fax: +44 117 9250612. E-mail: J.N.H., Jeremy.Harvey@bristol.ac.uk; M.N.R.A., mike.ashfold@bris.ac.uk.

† E-mail: J.Richley@bristol.ac.uk.

10.1021/jp906065v CCC: $40.75
Published on Web 09/24/2009

$$CH_x + CH_y(+M) \rightleftharpoons C_2H_{x+y}(+M) \quad (3a)$$

$$\rightleftharpoons C_2H_{x+y-1} + H \quad (3b)$$

$$\rightleftharpoons C_2H_{x+y-2} + H_2 \quad (3c)$$

The various C_2H_x species also interconvert through a series of H-shifting reactions analogous to eqs 1 and 2, with C_2H_2 the thermodynamically favored hydrocarbon at high T_{gas}. Similar recombination and H-shifting reactions can lead to formation of C_nH_x ($n > 2$) species, which grow in relative abundance as the input carbon mole fraction is increased.

Typical MW plasma enhanced (PE) CVD reactors encompass a very wide range of gas temperatures, ranging from ~3000 K (or even higher in the case of some UNCD growth) in the center of the plasma ball to not much above 300 K close to the water cooled reactor wall. Given such steep T_{gas} gradients, it follows that the total gas phase number densities, the H atom densities, the various hydrocarbon species densities, and thus the reaction rates for interconversion between these species, are all sensitive functions of location within the reactor. This complexity is further compounded by gas−surface reactions (at the growing diamond surface, and at the walls of the reactor) and by gas transport which, in MWPECVD reactors, is largely diffusive, and thus mass (and species) dependent. Notwithstanding this complexity, the latest reactor diagnosis and modeling are capable of providing reliable number densities for many of the more abundant gas phase species close above the growing surface, for a range of process conditions; illustrative results for environments appropriate for MCD[5] and UNCD[8] growth are listed in Table 1. Several notable features are evident in this table. C_2H_2 and H atoms are, respectively, the most abundant hydrocarbon and the most abundant radical species near the substrate surface in both environments, despite the very different C/H ratios in the input gas mixtures. The latter difference manifests itself clearly in the hydrocarbon radical densities, however. Under MCD growth conditions, CH_3 radicals account for >99% of the total C_1H_x ($x = 0-3$) radical density at $z =$ 0.5 mm above the center of the substrate surface whereas, under UNCD growth conditions, CH_3 radicals are predicted to account for only ~26% of $\sum_{x=0}^{3}[CH_x]$ and to be outnumbered by C atoms (by more than a factor of 2) and by heavier radical species like C_2H and C_3.

Some early studies proposed C_2H_2 as a likely diamond growth species[9] but most contemporary models regard CH_3 radicals as the key growth species. Most such modeling has focused on CH_3 addition to a radical site on the 2 × 1 reconstructed, H-terminated diamond {100} surface. Energetically plausible mechanisms have been identified for this addition, for the subsequent H atom abstraction (resulting in a pendant CH_2 group) and bond rearrangement steps that lead to eventual incorporation of the incident C_1 species[1,3,10−12] (the so-called "ring-opening/ring closing" and "trough bridging" mechanisms[13]), and for the migration of CH_2 groups along both the dimer chains and rows on the C{100}:H 2 × 1 surface.[12−15] The aim of the present work is to test further the assumption that such CH_3 radical initiated chemistry is necessarily the dominant route for C incorporation in all CVD diamond material. As noted earlier, the majority of surface atoms are H-terminated, and the present computational study explores the energetics (and thus the feasibility) of alternative C incorporation pathways initiated by radical insertions into C−H (and C−C) bonds on the C{100}:H 2 × 1 surface. As in the previous studies, the choice of the {100} surface is motivated by the fact that it is an important and frequently observed surface in many diamond samples grown by CVD, though we recognize that many of the observations reported here should apply to reactions at other surfaces also. The unsaturated CH_x ($x < 3$) species studied here can also add to radical sites on the surface. These radical−radical recombination steps presumably do not involve an energy barrier, as found, experimentally, for a range of gas phase alkyl recombination reactions[16] and, theoretically, in previous studies of CH_3 addition to radical sites on the diamond surface.[12] Such addition processes have not been studied in the present work, however. Under MCD growth conditions, at least, the low densities of such CH_x ($x < 3$) species near the growing diamond surface (relative to that of CH_3) suggests that their addition reactions are unlikely to make a significant contribution to diamond growth.

TABLE 1: Predicted Gas Temperature and Number Densities of H Atoms and Some of the More Abundant Carbon Containing Species at $z = 0.5$ mm above the Centre of the Substrate for (A) MCD Growth and (B) UNCD Growth[a]

	species density/cm^{-3}	
species	A: MCD $T_{gas} = 1305$ K	B: UNCD $T_{gas} = 1306$ K
H	8.2×10^{15}	3.4×10^{15}
CH_4	1.0×10^{15}	2.1×10^{11}
CH_3	1.1×10^{14}	1.3×10^{11}
$^3CH_2$	4.6×10^{11}	2.3×10^{9}
$^1CH_2$	1.1×10^{10}	7.9×10^{7}
CH	1.7×10^{10}	1.5×10^{9}
C	5.1×10^{10}	4.7×10^{11}
C_2H_6	1.0×10^{12}	3.2×10^{8}
C_2H_5	2.7×10^{11}	1.0×10^{9}
C_2H_4	4.8×10^{14}	4.0×10^{12}
C_2H_3	1.9×10^{13}	2.4×10^{12}
C_2H_2	1.1×10^{16}	2.2×10^{15}
C_2H	3.1×10^{10}	1.4×10^{12}
$C_2(X)$	1.5×10^{7}	3.2×10^{10}
$C_2(a)$	6.3×10^{7}	8.9×10^{10}
C_3	1.3×10^{13}	4.4×10^{14}
C_3H_2	2.1×10^{14}	8.9×10^{13}
C_4H_2	1.1×10^{14}	1.3×10^{14}

[a] Process conditions: (A) 4.4% CH_4/7% Ar/balance H_2, $p = 150$ Torr, $P = 1.5$ kW, absorbed power density Q_J ~20−40 W cm^{-3}, $T_{sub} = 973$ K (ref 5); (B) 0.5% CH_4/1% H_2/balance Ar, $p = 170$ Torr, $P = 0.7$ kW, absorbed power density Q_J ~9 W cm^{-3} above the substrate center, Q_J ~0.7 W cm^{-3} in the center of plasma core, $T_{sub} = 873$ K (ref 8).

II. Computational Details

Two families of calculations were performed in the present study. All reactions were investigated by density functional theory (DFT) methods using the small C_9H_{14} cluster employed in previous modeling studies of carbon[17] (and boron[18]) addition to an H-terminated, 2 × 1 reconstructed diamond {100} surface, and two variants of this cluster, as illustrated in Figure 1. One of these variants is obtained by replacing one of the surface H atoms in the C_9H_{14} cluster by a CH_3 group, the other by inserting a CH_2 group into the surface C−C dimer bond. These variants represent two of the structures implicated in the classic ring-opening/closing mechanism for carbon incorporation into the diamond {100} surface: structures **3** and **7** in ref 12. As Figure 1 shows, the three variants support no fewer than 5 distinguishable surface C−H bonds and 4 distinguishable C−C bonds. These are henceforth identified as HC1−HC5 and CC1−CC4 as labeled in Figure 1. Potential energy minima and transition

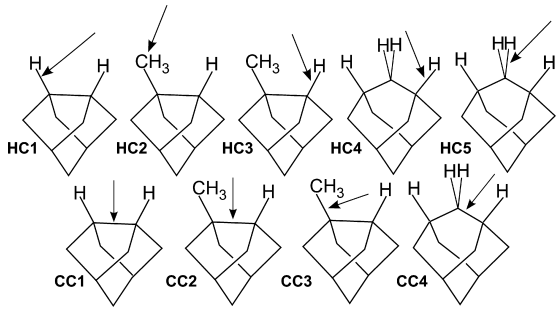

Figure 1. Basic C_9H_{14} cluster, and the two variants of this cluster, used in the QM investigations of the insertion of different C_1H_x species into C−H (HC1−HC5) and C−C (CC1−CC4) bonds on the diamond surface.

states (TSs) associated with insertion of various C_xH_y radical species into each of these C−H and C−C bonds were fully optimized using the standard B3LYP functional together with the 6-31G(d) basis set within the Gaussian03 program.[19] In some cases, there may be several isomeric TSs for insertion into the same bond, due to approach of the C_xH_y fragment from different angles. In such cases, the results described below correspond to the lowest energy pathway located. Vibrational frequencies were computed to confirm the nature of all stationary points, and to obtain estimates for the zero-point energy and for the entropy based on the rigid rotor/harmonic oscillator approximation. Single-point B3LYP energies were computed at the B3LYP/6-31G(d) geometries using the larger 6-311G(d,p) basis. All reported energies for entrance channel complexes ($E_{complex}$), transition states (E_{TS}), and the electronic energies of reaction (ΔE) are based on the B3LYP/6-311G(d,p) energies, with zero-point energy corrections calculated at the B3LYP/6-31G(d) level of theory.

Selected insertions were also studied by quantum mechanics/molecular mechanics (QM/MM) methods using the QoMMMa program,[20,21] as in our recent study of CH_3 addition to a radical site on the C{100}:H 2 × 1 surface.[12] Calculations for the QM region (typically a C_9 based cluster) were performed using Jaguar 5,[22] while interactions within the MM region were modeled using TINKER.[23] As before, the MM network involves a 5 × 9 × 4 slab (defined in terms of the number of C−C dimer bonds), the initial geometry of which is defined by the bulk diamond lattice points. Geometry optimization within the QM region involved use of the B3LYP density functional and the 6-31G(d) basis set, with the peripheral network described using the MM2 molecular mechanics protocol. Single point energies for the QM region were then calculated using the larger 6-311G(d,p) basis set. Approximate TSs for these reactions were identified by calculating the energy of the system at a series of values of a chosen reaction coordinate, q, which was either a key bond length or a combination of several bond lengths. Figure 2 serves to illustrate the constraints used when investigating C atom insertion into (a) C−H or (b) C−C bonds in the present QM/MM calculations. q in this case was restricted such that $q = (x + y - z)$, where x, y, and z are the separations between, respectively, nuclei 1 and 2, 2 and 3, and 1 and 3 and, for clarity of display, the MM region has been omitted from this depiction. A harmonic constraint was used to hold the system close to the desired value of the reaction coordinate. Single point energies calculated for the optimized QM region were combined with the optimized MM energies at each value along q, and the point of maximum energy along this curve then taken as the energy of the transition state. The spacing chosen for the values of q used in the mapping procedure is small enough that the estimated error on the approximate barrier heights in the QM/MM calculations is ≤5 kJ mol^{-1}. The reported QM/MM energies are again in kJ mol^{-1} and include a zero-point correction derived from the corresponding QM calculation.

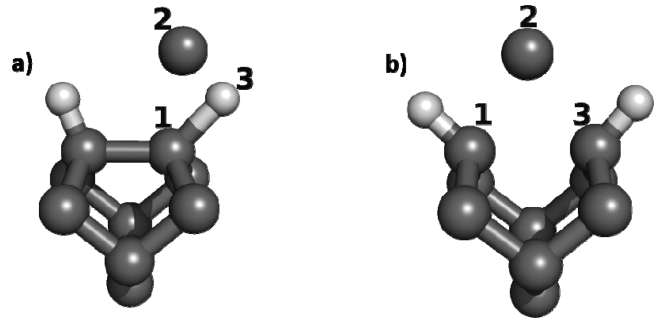

Figure 2. Illustrations of constraints used when investigating the insertion of a C_1H_x ($x \leq 2$) species into (a) C−H or (b) C−C bonds in the present QM/MM calculations. Note that, for display purposes, the MM region has been omitted from this depiction. q is restricted such that $q = (x + y - z)$, where x, y, and z are the separations between, respectively, nuclei 1 and 2, 2 and 3, and 1 and 3.

TABLE 2: B3LYP/6-311g(d,p)//B3LYP/6-31g(d) Energies (Including Zero Point Corrections Calculated at the B3LYP/6-31g(d) Level) for the Pre-Reaction Complexes ($E_{complex}$), Transition States (E_{TS}), and Reaction through to Final Products (ΔE) Associated with Insertion of a C(^{3}P) Atom into the Various C−C and C−H Bonds Illustrated in Figure 1[a]

insertion site	$E_{complex}$/kJ mol^{-1}	E_{TS}/kJ mol^{-1}	ΔE/kJ mol^{-1}
CC1	−21.2	90.5	−350.1
CC2	−21.0	115.9	−352.1
CC3	−14.6	166.3	−321.1
CC4	−29.2	156.8	−304.5
HC1	−21.1	−1.8	−305.3
HC2	−14.7	14.2	−289.6
HC3	−21.9	−0.2	−302.3
HC4	−29.4	−6.0	−300.6
HC5	−23.9	0.9	−294.2

[a] All energies are defined relative to those of the reactants.

III. Results and Discussion

This section describes elements of the calculated energy profiles for possible reactions of C_1H_x ($x = 0-2$), C_2H_x ($x = 0$, 1), and C_3 radical species with C−H and C−C bonds designed to mimic the C{100}:H 2 × 1 surface.

A. C(^{3}P) Atoms. Atomic carbon has been proposed previously as a potentially important species in diamond film growth.[24,25] Thermodynamic and multiplicity considerations dictate that gas phase C atoms adjacent to a growing diamond surface will be in their ground (^{3}P) state. The present QM studies find that insertion of a C(^{3}P) atom into the various C−H and C−C bonds shown in Figure 1 is, in all cases, highly exothermic and proceeds via a complex, in the entrance channel leading to the transition state region. As Table 2 shows, the calculated energy barriers to C(^{3}P) atom insertion into the various C−H bonds are small, and comparable to the well-depth of the entrance channel complex. Insertion of a C(^{3}P) atom into a C−C bond, in contrast, is calculated to involve a substantial energy barrier.

C(^{3}P) insertion into a C−H bond of methane was investigated also, to assess the reliability of the present DFT calculations. This reaction has been studied previously by Kim et al.,[26] at the CCSD(T)/6-311+G(3df,2p) level of theory. These workers

TABLE 3: B3LYP/6-311g(d,p)//B3LYP/6-31g(d) Energies (Including Zero Point Corrections Calculated at the B3LYP/6-31g(d) level) for $E_{complex}$, E_{TS}, and Reaction through to Final Products (ΔE) Associated with Insertion of a CH Radical into the Different C−C and C−H Bonds Illustrated in Figure 1[a]

insertion site	$E_{complex}$/kJ mol^{-1}	E_{TS}/kJ mol^{-1}	ΔE/kJ mol^{-1}
CC1	−32.1	82.7	−454.6
CC2	−28.7	110.7	−457.1
CC3	−28.7	171.2	−411.5
CC4	−40.7	157.0	−397.5
HC1	−36.3	−40.1	−413.2
HC2	−27.1	−28.6	−391.1
HC3	−36.2	−39.1	−409.1
HC4	−41.7	−42.4	−408.2
HC5	−36.2	−38.3	−403.8

[a] All energies are defined relative to those of the reactants.

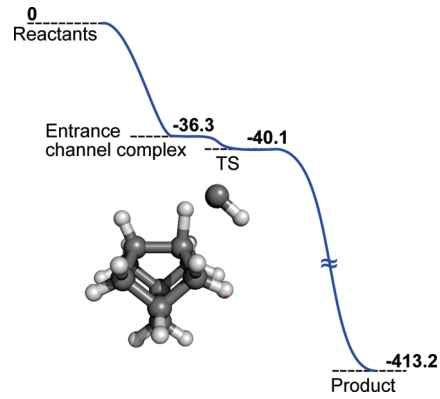

Figure 3. Minimum energy path for CH radical insertion into site HC1 (B3LYP/6-311g(d,p)//B3LYP/6-31g(d) energies (in kJ mol^{-1}, including zero point corrections calculated at the B3LYP/6-31g(d) level)) along with the TS structure returned by the QM calculation.

identified a shallow minimum in the entrance channel ($E_{complex}$ = −3.3 kJ mol^{-1}), a TS at E_{TS} = 51 kJ mol^{-1} and a reaction exothermicity ΔE = −268 kJ mol^{-1}. The present B3LYP/6-311g(d,p)//B3LYP/6-31g(d) calculations return an essentially identical TS geometry and energies (again including zero point corrections) that are in reassuringly good accord: $E_{complex}$ = −4.6 kJ mol^{-1}, E_{TS} = 34.7 kJ mol^{-1}, and ΔE = −285 kJ mol^{-1}.

C(^{3}P) atom insertion into a surface C−H bond was also investigated by QM/MM methods. The QM/MM structures obtained throughout this study were usually very similar to those obtained with the QM model, justifying the use of the latter. The small number of significant differences, due essentially to steric effects from the remainder of the diamond surface, are discussed below. The energies returned by QM/MM calculations for C(^{3}P) atom insertion into a C−H bond on the pristine C{100}:H 2 × 1 surface (equivalent to HC1 in Figure 1) agree well with the QM calculations. Again, the calculations reveal an entrance channel complex with an energy 23 kJ mol^{-1} lower than that of the reactants, followed by an activation barrier 0.2 kJ mol^{-1} below the reactant energy. Readers should note that the extended diamond surface used in the QM/MM calculations constrains the TS for this insertion more tightly than in the QM calculations employing the C_9H_{14} cluster. In the QM/MM case, the minimum energy pathway involves a TS as shown in Figure 2a in which the critical internuclear separations between atoms 1 and 2, 2 and 3, and 3 and 1 are, respectively, 1.94, 1.17, and 1.41 Å. In terms of the bond lengths, this is similar to that found for the QM TS (where the corresponding distances are 1.80, 1.17, and 1.57 Å). The preferred angle of approach of the C atom toward the C−H bond is different in the two cases, however; the lowest energy pathway in the QM calculation has the incident C atom approaching from the trough side of the C−H bond (reflecting the lack of steric hindrance when using the small C_9H_{14} cluster model).

B. CH Radicals. Rate constants for the reaction of ground ($X^2\Pi$) state CH radicals with CH_4 and with several larger hydrocarbons have been measured, at a range of temperatures,[27−30] and reaction mechanisms deduced by complementary quantum chemical modeling.[31,32] All support the view that CH radical insertion into a C−H bond in an alkane is a barrierless process.

As Table 3 shows, this behavior extrapolates to the case of C−H bonds on a diamond surface also. The present QM calculations show that CH radical insertion into each of structures HC1−HC5 proceeds via an entrance channel complex and subsequent passage over a TS that, in all cases, lies well below the reactant energy, as shown in Figure 3 (for the specific case of CH radical insertion into HC1). The displayed TS structure is a consequence of orbital interactions similar to those invoked when describing the insertion of singlet carbenes into C−H bonds,[33] viz. bonding interactions between the empty p orbital of the radical and the filled σ orbital of the surface C−H bond, and between the highest doubly occupied orbital of the radical and the empty σ^* orbital of the bond into which insertion occurs. Higher level single point calculations using the 6-311g(d,p) basis set cast doubt as to whether these reactions involve a TS in the conventional sense. After zero-point corrections are included, the various TSs are actually calculated to lie slightly lower in energy than the corresponding entrance channel complex and, in all cases, to be rather insensitive to the azimuthal location of the center of mass of the incoming CH radical relative to the surface C−H bond into which insertion is to occur. CH radicals also form a complex in the entrance channel leading to insertion into a C−C bond but, as Table 3 shows, the subsequent barrier to reaction is prohibitive.

CH radical insertion into C−H and C−C bonds on the C{100}:H 2 × 1 surface was investigated by the QM/MM methods also, using constraints similar to those described in Figure 2. The present calculations failed to reveal any obvious energy barrier to inserting a CH radical into a surface C−H bond; if a barrier exists, it is very small, and comparable to the numerical uncertainties associated with calculations performed at different q. As with the C(^{3}P) atom insertion discussed above, the minimum energy pathway returned by the QM/MM studies has the CH radical approaching the C−H bond of interest from above the C−C dimer bond (and with the radical bond near perpendicular to this dimer bond) rather than from the trough side, as shown in Figure 3, again, presumably, as a result of local steric interactions associated with the extended surface structure. QM/MM investigations of CH radical insertion into a surface C−C bond led to a TS structure very similar to that found in the QM calculation, with an energy barrier of ∼77 kJ mol^{-1}, slightly smaller than the QM value, perhaps due to the stretching effect on the dimer bond exerted by the diamond matrix.

C. CH_2 Radicals. The very different reactivities of singlet and triplet carbenes are well-known.[34] Singlet carbenes have the appropriate electronic configuration (i.e., a suitable doubly occupied donor orbital and an empty, low-lying acceptor orbital) to insert into available C−H bonds, whereas the triplet species is more likely to abstract the H atom. Methylene, the simplest carbene, has a triplet ($\tilde{X}^3B_1$) ground state (henceforth identified simply as $^3CH_2$). Its first excited singlet state, (the $\tilde{a}^1A_1$ state, henceforth represented as $^1CH_2$) lies only ∼0.4 eV higher in

TABLE 4: B3LYP/6-311g(d,p)//B3LYP/6-31g(d) Energies (Including Zero Point Corrections Calculated at the B3LYP/6-31g(d) Level) for E_{TS} and ΔE for Insertion of a $^1CH_2$ Radical into the Different C−C and C−H Bonds Illustrated in Figure 1[a]

insertion site	E_{TS}/kJ mol^{-1}	ΔE/kJ mol^{-1}
CC1	122.2	−487.5
CC2	149.6	−476.6
CC3	200.2	−433.4
CC4	195.9	−408.1
HC1	−15.3	−449.6
HC2	−5.8	−433.4
HC3	−9.3	−443.7
HC4	−22.0	−438.7
HC5	−15.8	−437.7

[a] All energies are defined relative to those of the reactants.

energy. If these two states were in local thermodynamic equilibrium at the gas temperature close to the substrate surface (T_{gas} = 1305 K, Table 1), then only ∼1% of the methylene radicals would be present as $^1CH_2$. The literature contains many theoretical studies of $^1CH_2$ radical insertions into both C−H[33,35,36] and C−C[37,38] bonds in isolated hydrocarbon molecules. The former processes generally exhibit low energy barriers, while the activation energies for $^1CH_2$ radical insertion into C−C bonds are generally much larger. This difference is confirmed experimentally, for example, in the much faster relative rates of $^1CH_2$ radical insertions into C−H bonds as compared with C−C bonds.[39]

The present QM investigations identified TSs for $^1CH_2$ radical insertion into the various C−H bonds HC1−HC5. As Table 4 shows, all are calculated to be lower in energy than the reactants. Incorporation should thus be efficient and rapid. In fact, insertion should be even more facile than suggested by this description, since we find no barrier to addition when bringing the CH_2 moiety up to a given C−H bond with an alternative orientation to that found in the identified TS. The absence of barrier for this alternative (and thus implicitly more favorable) approach geometry also explains our inability to localize minima associated with entrance channel complexes for the TSs listed in Table 4. This reflects the fact that, upon relaxing the geometry away from the TS and toward the putative entrance channel complex, the CH_2 fragment can reorient in such a way as to lead to barrierless insertion along an isomeric reaction path into either the same or a different C−H bond; attempted optimization from the product or reactant side of the TS thereby leads directly to an inserted species. Such a finding accords with the results of Bach et al.,[33] who located two different TSs for $^1CH_2$ insertion into C−H bonds when using Hartree−Fock theory (which traditionally overestimates the corresponding barrier heights). At higher levels of theory, however, the lower of the two barriers disappeared, again suggesting that addition involving one of the two possible CH_2 orientations is barrierless. This interpretation is reinforced by the results of our companion QM/MM study, wherein the constrained optimizations along the reaction coordinate show no barrier to reaction when the $^1CH_2$ fragment approaches the C−H bond on the C{100}:H 2 × 1 surface with the more favorable orientation.

$^1CH_2$ radical insertion into C−C bonds has been investigated also, by both QM and QM/MM methods. The former calculations returned TSs with high barriers (Table 4), implying that such reactions are unlikely to be important in diamond CVD. The QM/MM calculations also predict a barrier to addition, of ∼106 kJ mol^{-1}, with a similar geometry to that found in the QM investigations.

$^3CH_2$ radicals lack the necessary empty acceptor orbital to participate in insertion reactions but can add to surface radical sites, in a manner analogous to the classic addition of CH_3 radicals to a growing diamond surface.[3] $^3CH_2$ radicals can also abstract the H atom from a surface C−H bond. B3LYP/6-311g(d,p)//B3LYP/6-31g(d) calculations on the QM model system, including zero point correction calculated at the B3LYP/6-31g(d) level, show that the energy barrier for abstraction of an HC1-type H atom by an incident $^3CH_2$ radical is only 14.3 kJ mol^{-1}. We note that the products of this abstraction process are a surface radical site and a gas phase CH_3 radical proximate to the surface. These could recombine, in principle at least, to yield the same surface bound pendant CH_3 group as that implicated in traditional (CH_3 based) models of MCD growth and as would be formed by $^1CH_2$ radical insertion into a surface C−H bond.

D. C_2 Radicals. The C_2 radical has a $^1\Sigma_g^+$ ground state and a low lying $a^3\Pi_u$ excited state, henceforth represented as $^1C_2$ and $^3C_2$. The energy separation between these states is only 0.089 eV, and the latter has a 6-fold electronic degeneracy. If these two states are in local thermodynamic equilibrium immediately above the growing diamond surface at T_{gas} = 1305 K, ∼73% of all C_2 radicals would be present as triplets. $^3C_2$ radicals do not participate in insertion reactions but will add to radical sites on the growing surface and can also contribute to surface activation by abstracting the H atom from a surface C−H bond. $^1C_2$ radicals, in contrast, do insert into C−H bonds. The Argonne group have previously reported QM studies of $^1C_2$ radical insertion into C−H bonds in methane[40] and in a C_9H_{14} cluster,[41] at several different levels of theory. The higher-level calculations suggest a negligible energy barrier in the former insertion, and this result was assumed to extend to the latter process also. The present QM calculations support this view, inasmuch that we were unable to locate a TS for $^1C_2$ insertion into, for example, HC1. This insertion reaction was found to be exothermic (ΔE = −477.7 kJ mol^{-1}), in excellent accord with the value of Gruen et al. (ΔE = −480.6 kJ mol^{-1}, calculated at the B3LYP/6-31G* level[41]). The present QM study finds that rearrangement of the resulting vinylidene-like appendage to an acetylene group is also exothermic (ΔE = −198 kJ mol^{-1}). The transition state for this rearrangement was located and, with correction for zero-point energy, the single-point energy with the large basis set leads to a predicted E_{TS} of −4.9 kJ mol^{-1}, implying that any energy barrier associated with this process must be very small.

The QM/MM studies return very similar energies, and find no activation barrier to $^1C_2$ radical insertion into a C−H bond on the C{100}:H 2 × 1 surface. The resulting structure, with the vinylidene-like appendage, is calculated to be 468 kJ mol^{-1} more stable than the reactants. Again, the subsequent rearrangement of the pendant group to a surface bound C≡CH acetylene group is found to have a very low barrier (E_{TS} ∼1 kJ mol^{-1}, calculated at the B3LYP/6-31G*:MM2 level), and to be exothermic (ΔE = −201.7 kJ mol^{-1}). Here too, single point energy calculations using the larger basis set suggest that the TS actually lies lower in energy than the vinylidene-like intermediate. Given this low (or nonexistent) barrier, we suggest rearrangement (to form the surface acetylene group) as the dominant fate of the vinylidene-like appendage formed by $^1C_2$ insertion into a surface C−H bond, given the larger energy barriers of the possible rival pathways (e.g., cyclobutene-like ring formation, or rearrangement and insertion into the C−C dimer bond) suggested by Gruen et al.[41]

E. C_2H Radicals. Table 1 suggests that C_2H radicals will be more abundant than any of the C_1H_x ($x \leq 3$) species under UNCD growth conditions. This radical lacks the necessary empty acceptor orbital to participate in insertion reactions, however, and its principal role at the growing diamond surface will be to abstract a surface terminating H atom, forming gas phase C_2H_2. Such a conclusion accords with earlier QM studies of the $C_2H + C_2H_6$ reaction,[42] which found a small energy barrier ($E_{TS} \sim 3$ kJ mol^{-1}) to abstracting an H atom, but a large barrier ($E_{TS} \sim 220$ kJ mol^{-1}) to radical insertion into one of the C−H bonds.

F. C_3 Radicals. Table 1 indicates that C_3 is one of the more abundant carbon-containing radical species in most diamond growing environments. QM calculations for the reaction of a ground ($^1\Sigma_g^+$) state C_3 radical with structure HC1 show that the minimum energy path involves insertion into a C−H bond, that the process involves a significant energy barrier ($E_{TS} \sim 105$ kJ mol^{-1} at the B3LYP/6-31g(d) level), and that it is exothermic: $\Delta E = -231$ kJ mol^{-1}.

IV. Implications for Diamond CVD

We preface this discussion with a summary of the likely probabilities and time scales of some of the key reaction steps involved in diamond CVD. The flux of atomic hydrogen to the surface under the representative MCD growth conditions shown in Table 1 is $\sim 10^{19}$ cm^{-2} s^{-1} (and $\sim 4 \times 10^{18}$ cm^{-2} s^{-1} for the UNCD growth conditions). Given a surface density of $\sim 2 \times 10^{15}$ C atoms per cm^2 (representative of the diamond (100) surface), each surface C atom will thus experience $\sim 10^4$ collisions with incident gas phase H atoms per second, thereby maintaining a surface terminated with C−H bonds in steady state with a fraction of radical sites. This fraction depends on T_{sub} but is typically considered to be of the order of a few percent.[43] The probability of an incident gas phase H atom abstracting a surface hydrogen and forming molecular H_2 at the substrate temperatures of interest is ~ 0.1, while the probability for an incident H atom recombining with a radical site is near unity. Thus, though the fraction of surface radical sites is in steady state, it is important to recognize the dynamic status of each surface C atom, whereby its surface terminating H atom frequently exchanges with the gas phase. As Table 1 shows, the density of C_1H_x ($x \leq 3$) species near the surface under MCD growth conditions is 2 orders of magnitude less than the H atom density. The frequency with which an incident CH_3 radical encounters a given surface atom while in a reactive (i.e., radical) state under such conditions is thus only ~ 10 s^{-1}. Full incorporation of this incident radical into the diamond lattice via, for example, the ring-opening/ring closing mechanism, requires a further H atom abstraction, a sequence of surface rearrangement steps, and an eventual H atom addition, but the CH_3 radical addition represents the rate limiting step in the absence of significant carbon etching processes.[12,13]

The present study shows that C(^{3}P), CH, $^1CH_2$, and $^1C_2$ radicals can all insert into C−H bonds, via reaction pathways that are essentially barrierless. Here it is necessary to sound one note of caution. The QM and QM/MM calculations return (zero-point corrected) electronic energies of reaction, ΔE, but the most important quantity determining reaction rates and equilibria is the change in Gibbs energy, $\Delta_r G$. With $T_{sub} \sim 1000$ K, entropic contributions to $\Delta_r G$ can be significant, particularly in reactions, as here, that involve the loss or formation of a gas phase species. By way of example, the present QM calculations show that $\Delta_r S$ for insertion of a C(^{3}P) atom into a surface C−H bond will be ~ -116 J K^{-1} mol^{-1}. Viewed in terms of a free energy surface, the exoergicity of this reaction will thus be reduced by ~ 116 kJ mol^{-1} and, more importantly, the transition state free energy (defined relative to reactants) will be raised by ~ 107 kJ mol^{-1}. Similar arguments will apply to the insertion of carbon containing radicals into a C−C bond. Given that the present calculations return substantial activation barriers for all C−C bond insertions, and that inclusion of entropic effects will only serve to increase these barriers further, we conclude that the insertion of carbon containing radicals into C−C bonds is not important in diamond CVD.

Thus we focus on C(^{3}P), CH, $^1CH_2$, and $^1C_2$ radical insertions into surface C−H bonds. The latter are the majority surface species, outnumbering radical sites by a factor of 10 or more in almost all diamond CVD environments. Notwithstanding the high fraction of such surface sites, however, the low abundance of the relevant gas phase C_1H_x ($x \leq 2$) and $^1C_2$ radicals relative to CH_3 under typical MCD growth conditions (see Table 1) suggests that such insertion reactions can only make, at most, a small contribution to the total carbon incorporated within a growing MCD film. Such reactions do offer an alternative route to introducing C atoms at the growing surface, however, and thus might provide a means of filling the atom-sized voids found in contemporary Monte Carlo simulations of MCD growth (which neglect such insertions).[15]

As Table 1 shows, the relative abundances of C(^{3}P) atoms and CH_3 radicals at the growing surface of a UNCD film are very different. The CH_3 radical density under these conditions is some 3 orders of magnitude lower than in the case of MCD growth, and C(^{3}P) atoms are predicted to be the dominant C_1H_x species. This, together with the fact that most surface atoms will be C−H terminated, implies that insertion of C(^{3}P) atoms into surface C−H bonds is likely to play a significant role in the nucleation and growth of UNCD films. Insertion results in a surface-bound CH group. Addition of a gas phase H atom will result in a pendant CH_2 group, that is central to many of the elementary growth mechanisms identified on a C{100}:H 2×1 surface, e.g., incorporation via the ring-opening/ring closing and dimer trough bridging mechanisms, and in the migration of surface carbon atoms.[12] A C(^{3}P) atom is, of course, also able to add to a surface radical site. Under UNCD growth conditions, therefore, an incident C atom can be accommodated at *any* surface site, whether H terminated or not, which provides an (at least partial) explanation for the high nucleation density and the very small grain size in the resulting material.

$^1C_2$ radicals can also insert into surface C−H bonds via a barrierless PES and can also add to surface radical sites. As commented earlier, the majority of gas phase C_2 radicals adjacent to a growing UNCD surface are likely to be in the triplet state. Table 1 suggests that the $^1C_2$ radical density in the gas phase proximate to the growing diamond surface will be at least 1 order of magnitude lower than that of C(^{3}P) atoms. $^1C_2$ radical insertion (or addition) will contribute two carbon atoms to the surface, but their subsequent hydrogenation (whether as a pendant vinylidene or acetylene group) will render them vulnerable to subsequent loss by β-scission, as a gas phase C_2H_2 or C_2H_4 molecule.[1] Similar arguments would likely apply in the case of any C_3 radical insertions. Thus, within the context of the insertion reactions considered here, C(^{3}P) atoms appear to be plausible growth species under conditions typically used for MWPECVD of UNCD films.

Finally, we note that several other atoms (e.g., B, and electronically excited O(^{1}D) and N(^{2}D) atoms) and radicals (e.g., BH) possess the appropriate combination of full donor and empty acceptor orbitals required for insertion into, particularly,

C−H bonds. Even with suitable nitrogen or oxygen doped gas mixtures, the density of electronically excited species near the substrate surface will be low at the pressures used in diamond CVD. The B containing species are of relevance, however, given the growing applicability of B doped CVD diamond material.[44] Previous QM studies have addressed the energetics of BH_x ($x \leq 3$) radical additions to the C{100}:H 2 × 1 surface;[18] their insertion reactions will be the subject of a future study.

V. Conclusions

Addition of a gas phase CH_3 radical to a surface radical site is regarded as the rate limiting step in most contemporary modeling of diamond growth by CVD methods. Here we have used two computational approaches to explore the potential energy profiles of gas-surface reactions involving alternative carbon containing species known to be present in the gas phase proximate to the growing diamond surface (C atoms, and CH, CH_2, C_2, C_2H, and C_3 radicals). The QM (DFT) calculations employed a small C_9H_{14} cluster as a mimic of the C{100}:H 2 × 1 surface. The hybrid QM/MM calculations used a similar cluster (modeled by QM methods), embedded in a much more extensive network of atoms (a 5 × 9 × 4 slab, defined in terms of the number of C−C dimer bonds) which is treated by molecular mechanics. Both sets of calculations suggest that the minimum energy pathways for inserting a C atom, or a CH, $^1C_2$, or $^1CH_2$ radical into a surface C−H bond are essentially barrierless, whereas the barrier to inserting any of the investigated species into a surface C−C bond is prohibitively high. As a reactant, therefore, the diamond surface shows many behavioral similarities to an alkane; in both cases, an incident species presenting a filled σ orbital and an empty p(π) orbital can insert readily into C−H bonds. Insertion reactions involve removal of a gas phase species and are thus entropically disfavored. The majority of surface C atoms under typical CVD conditions are H-terminated, however, and the present calculations suggest that insertion reactions (particularly those involving $C(^3P)$ atoms) may well contribute to the renucleation and growth of UNCD films.

Acknowledgment. We are grateful to EPSRC for the award of a research grant and studentship (to J.C.R.), to Element Six Ltd. for financial support and the long-term loan of the MWPECVD reactor, and to colleagues Drs. A. Cheesman (now at Szeged University) and Yu. A. Mankelevich (Moscow State University) for their many contributions to the work described here.

References and Notes

(1) Goodwin, D. G.; Butler, J. E. In *Handbook of Industrial Diamonds and Diamond Films*; Prelas, M. A., Popovici, G., Bigelow, L. G., Eds.; Marcel Dekker: New York, 1998; pp 527−81 and references therein.

(2) Petrini, D.; Larsson, K. *J. Phys. Chem. C.* **2008**, *112*, 14367, and references therein.

(3) Butler, J. E.; Mankelevich, Y. A.; Cheesman, A.; Ma, J.; Ashfold, M. N. R. *J. Phys. Condens. Matter* **2009**, *21*, 364201, and references therein.

(4) Ma, J.; Cheesman, A.; Ashfold, M. N. R.; Hay, K. G.; Wright, S.; Langford, N.; Duxbury, G.; Mankelevich, Y. A. *J. Appl. Phys.* **2009**, *106*, 033305.

(5) Ma, J.; Richley, J. C.; Ashfold, M. N. R.; Mankelevich, Y. A. *J. Appl. Phys.* **2008**, *104*, 103305.

(6) Ma, J.; Ashfold, M. N. R.; Mankelevich, Y. A. *J. Appl. Phys.* **2009**, *105*, 043302.

(7) Mankelevich, Y. A.; Ashfold, M. N. R.; Ma, J. *J. Appl. Phys.* **2008**, *104*, 113304.

(8) Fox, O. J. L.; Ma, J.; May, P. W.; Ashfold, M. N. R.; Mankelevich, Yu. A. *Diamond Relat. Mater.* **2009**, *18*, 750.

(9) Skokov, S.; Weiner, B.; Frenklach, M. *J. Phys. Chem.* **1995**, *99*, 5616, and references therein.

(10) Skokov, S.; Weiner, B.; Frenklach, M. *J. Phys. Chem.* **1994**, *98*, 8; **1994**, *98*, 7073.

(11) Tamura, H.; Zhou, H.; Hirano, Y.; Takami, S.; Kubo, M.; Belosludov, R. V.; Miyamoto, A.; Imamura, A.; Gamo, M. N.; Ando, T. *Phys. Rev. B.* **2000**, *62*, 16995.

(12) Cheesman, A.; Harvey, J. N.; Ashfold, M. N. R. *J. Phys. Chem. A* **2008**, *112*, 11436.

(13) Garrison, B. J.; Dawnkaski, E. J.; Srivastava, D.; Brenner, D. W. *Science* **1992**, *255*, 835.

(14) Frenklach, M.; Skokov, S. *J. Phys. Chem. B.* **1997**, *101*, 3025.

(15) Netto, A.; Frenklach, M. *Diamond Relat. Mater.* **2005**, *14*, 1630.

(16) See, for example: Knyazev, V. D.; Slagle, I. R. *J. Phys. Chem. A* **2001**, *105*, 6490.

(17) Kang, J. F.; Musgrave, C. B. *J. Chem. Phys.* **2000**, *113*, 7582.

(18) Cheesman, A.; Harvey, J. N.; Ashfold, M. N. R. *Phys. Chem. Chem. Phys.* **2005**, *7*, 1121.

(19) Frisch, M. J.; Trucks, G. W.; Schlegel, H. B.; Scuseria, G. E.; Robb, M. A.; Cheeseman, J. R.; Montgomery, J. A., Jr.; Vreven, T.; Kudin, K. N.; Burant, J. C.; Millam, J. M.; Iyengar, S. S.; Tomasi, J.; Barone, V.; Mennucci, B.; Cossi, M.; Scalmani, G.; Rega, N.; Petersson, G. A.; Nakatsuji, H.; Hada, M.; Ehara, M.; Toyota, K.; Fukuda, R.; Hasegawa, J.; Ishida, M.; Nakajima, T.; Honda, Y.; Kitao, O.; Nakai, H.; Klene, M.; Li, X.; Knox, J. E.; Hratchian, H. P.; Cross, J. B.; Adamo, C.; Jaramillo, J.; Gomperts, R.; Stratmann, R. E.; Yazyev, O.; Austin, A. J.; Cammi, R.; Pomelli, C.; Ochterski, J. W.; Ayala, P. Y.; Morokuma, K.; Voth, G. A.; Salvador, P.; Dannenberg, J. J.; Zakrzewski, V. G.; Dapprich, S.; Daniels, A. D.; Strain, M. C.; Farkas, O.; Malick, D. K.; Rabuck, A. D.; Raghavachari, K.; Foresman, J. B.; Ortiz, J. V.; Cui, Q.; Baboul, A. G.; Clifford, S.; Cioslowski, J.; Stefanov, B. B.; Liu, G.; Liashenko, A.; Piskorz, P.; Komaromi, I.; Martin, R. L.; Fox, D. J.; Keith, T.; Al-Laham, M. A.; Peng, C. Y.; Nanayakkara, A.; Challacombe, M.; Gill, P. M. W.; Johnson, B.; Chen, W.; Wong, M. W.; Gonzalez C.; Pople, J. A. *Gaussian 03*, revision B.04; Gaussian, Inc.: Pittsburgh PA, 2003.

(20) Harvey, J. N. *Faraday Discuss.* **2004**, *127*, 165.

(21) Tsipis, A. C.; Orpen, A. G.; Harvey, J. N. *Dalton Trans.* **2005**, 2849.

(22) Jaguar, Schrödinger Inc., Portland, OR, 2000.

(23) Ponder, J. W. TINKER: Software Tools for Molecular Design, v4.0; Saint Louis, MO, 2003.

(24) Yu, B. W.; Girshick, S. L. *J. Appl. Phys.* **1994**, *75*, 3914.

(25) Joe, R.; Badgwell, T. A.; Hauge, R. H. *Diamond Relat. Mater.* **1998**, *7*, 1364.

(26) Kim, G. S.; Nguyen, T. L.; Mebel, A. M.; Lin, S. H.; Nguyen, M. T. *J. Phys. Chem. A* **2003**, *107*, 1788.

(27) Butler, J. E.; Fleming, J. W.; Goss, L. P.; Lin, M. C. *Chem. Phys.* **1981**, *56*, 355.

(28) Berman, M. R.; Lin, M. C. *Chem. Phys.* **1983**, *82*, 435.

(29) Galland, N.; Caralp, F.; Hannachi, Y.; Bergeat, A.; Loison, J. C. *J. Phys. Chem. A* **2003**, *107*, 5419.

(30) Loison, J. C.; Bergeat, A.; Caralp, F.; Hannachi, Y. *J. Phys. Chem. A* **2006**, *110*, 13500.

(31) Wang, Z. X.; Huang, M. B.; Liu, R. Z. *Can. J. Chem.* **1997**, *75*, 996.

(32) Wang, Z. X.; Huang, M. B. *J. Chem. Soc., Faraday Trans* **1998**, *94*, 635.

(33) Bach, R. D.; Su, M. D.; Aldabbagh, E.; Andres, J. L.; Schlegel, H. B. *J. Am. Chem. Soc.* **1993**, *115*, 10237.

(34) Kirmse, W. *Carbene Chemistry*, 2nd ed.; Academic: New York, 1971.

(35) Gordon, M. S.; Gano, D. R. *J. Am. Chem. Soc.* **1984**, *106*, 5421.

(36) Ramalingam, M.; Ramasami, K.; Venuvanalingam, P.; Sethuraman, V. *J. Mol. Struct. (THEOCHEM)* **2005**, *755*, 169.

(37) Gordon, M. S.; Boatz, J. A.; Gano, D. R.; Friedrichs, M. G. *J. Am. Chem. Soc.* **1987**, *109*, 1323.

(38) Gano, D. R.; Gordon, M. S.; Boatz, J. A. *J. Am. Chem. Soc.* **1991**, *113*, 6711.

(39) Becerra, R.; Frey, H. M. *Chem. Phys. Lett.* **1987**, *138*, 330.

(40) Horner, D. A.; Curtiss, L. A.; Gruen, D. M. *Chem. Phys. Lett.* **1995**, *233*, 243.

(41) Gruen, D. M.; Redfearn, P. C.; Horner, D. A.; Zapol, P.; Curtiss, L. A. *J. Phys. Chem. B* **1999**, *103*, 5459.

(42) Ceursters, B.; Nguyen, H. M. T.; Nguyen, M. T.; Peeters, J.; Vereecken, L. *Phys. Chem. Chem. Phys.* **2001**, *3*, 3070.

(43) Butler, J. E.; Woodin, R. L. *Philos. Trans. R. Soc. Lond.* **1993**, *342*, 15.

(44) Deneuville, A. *Semiconductors Semimetals* **2003**, *76*, 183, and references therein.

JP906065V